



Size and Shape Control of Metal Nanoparticles for Reaction Selectivity in Catalysis

Kwangjin An and Gabor A. Somorjai*^[a]

A nanoparticle with well-defined surfaces, prepared through colloidal chemistry, enables it to be studied as a model heterogeneous catalyst. The colloidal synthetic approach provides versatile tools to control the size and shape of nanoparticles. Traditional nucleation and growth mechanisms have been utilized to understand how nanoparticles can be uniformly synthesized and unprecedented shapes can be controlled. Now, the size of metal particles can be controlled to cluster regimes by using dendrimers. By using seeds and foreign atoms, specific synthetic environments such as seeded growth and crystal

overgrowth can be induced to generate various shaped mono- or bi-metallic, core/shell, or branched nanostructures. For green chemistry, catalysis in 21st century is aiming for 100% selectivity to produce only one desired product at high turnover rates. Recent studies on nanoparticle catalysts clearly demonstrate size and shape dependent selectivity in many catalytic reactions. By combining in situ surface characterization techniques, real-time monitoring of nanoparticles can be performed under reaction environments, thus identifying several molecular factors affecting catalytic activity and selectivity.

1. Introduction

Over the last few decades, the field of nanotechnology has exponentially expanded and has been incorporated into many areas of science, including biology, environmental science, and energy research.^[1–2] With the rising development for applications in nanotechnology, synthetic strategies for nanomaterials have also evolved to meet the technological demands. Among these nanomaterials, metal nanoparticles with well-defined surfaces have attracted significant attention in many research areas, owing to their extraordinary catalytic properties.^[3] Industrial heterogeneous catalysts, composed of metal nanoparticles, have been widely utilized owing to their high surface to volume ratio. However, the broad size distribution of these particles, and the lack of structural characterization have been obstacles in understanding their structure-dependent catalytic activity and selectivity.^[4] Recent progress in nanoparticle syntheses, based on a colloidal chemistry, attains a completeness of artistic achievement. Now, the size of nanoparticles can be controlled on an atomic-scale, preserving the high uniformity with an extremely narrow size distribution ($\sigma_r \leq 5\%$). Recently, it became possible to reduce the particle size down to cluster ranges of less than one nanometer.^[5] By means of versatile, colloidal synthetic approaches, a variety of shapes have also been achieved so far, including not only simple shapes (sphere, cube, tetrahedron, octahedron, decahedron, and icosahedrons), but also 1- or 2-dimensional shapes (rod, wire, plate, disc, triangular- and hexagonal-plate, and more complicated bi-pyramid, tetrapods, and hyper-branched structures) (Figure 1).^[6–7] Nanoparticles with high surface areas can provide more active sites to lower activation energy for catalytic reactions, and unique surface structures—such as steps, kinks, and terraces—to influence reaction pathways leading to product selectivity. Recent studies show that turnover rates and selectivity of catalytic reactions can be influenced strongly by the

size and shape of nanoparticles, as their surface structures and active sites can be tailored at the molecular level.^[8]

In this review article, we highlight how size and shape of metal nanoparticles produced by colloidal chemistry can be controlled and their specific morphologies are utilized and optimized in many catalytic applications. Because a surface to volume ratio is enhanced sharply as a particle size is decreased below 5 nm, as an important goal in catalytic chemistry, the size controlling strategies of nanoparticles will be suggested in a size regime of 1–10 nm.^[8] Substantial achievement in the synthesis of various noble metal nanoparticles has been made by Younan Xia's group who compiled the shape control strategies.^[6] In this review, we discuss the concepts and examples of producing shape-controlled metal nanoparticles from their works.^[6–7] However, we focus much of the review on the structure-dependent selectivity of Pt nanoparticles for heterogeneous catalysis. In addition to Pt, novel metals including Pd, Rh, and Ru have been widely used as prominent catalysts for industrial applications, which include production of a high-octane gasoline, and chemical productions as well as cracking, refining, and reforming of petroleum.^[4] Therefore, the size and shape control strategies of the Pt group metal nanoparticles will be focused on reactions important in conversion of hydrocarbons. First, the basic concepts of colloidal synthesis of monodispersed nanoparticles are introduced. In the following sections, we describe several strategies for controlling size and shape of metal nanoparticles and advanced in situ and ex situ

[a] Dr. K. An, Prof. G. A. Somorjai
Department of Chemistry
University of California and Chemical Sciences and Materials
Sciences Divisions, Lawrence Berkeley National Lab.
Berkeley, California 94720 (USA)
E-mail: somorjai@berkeley.edu

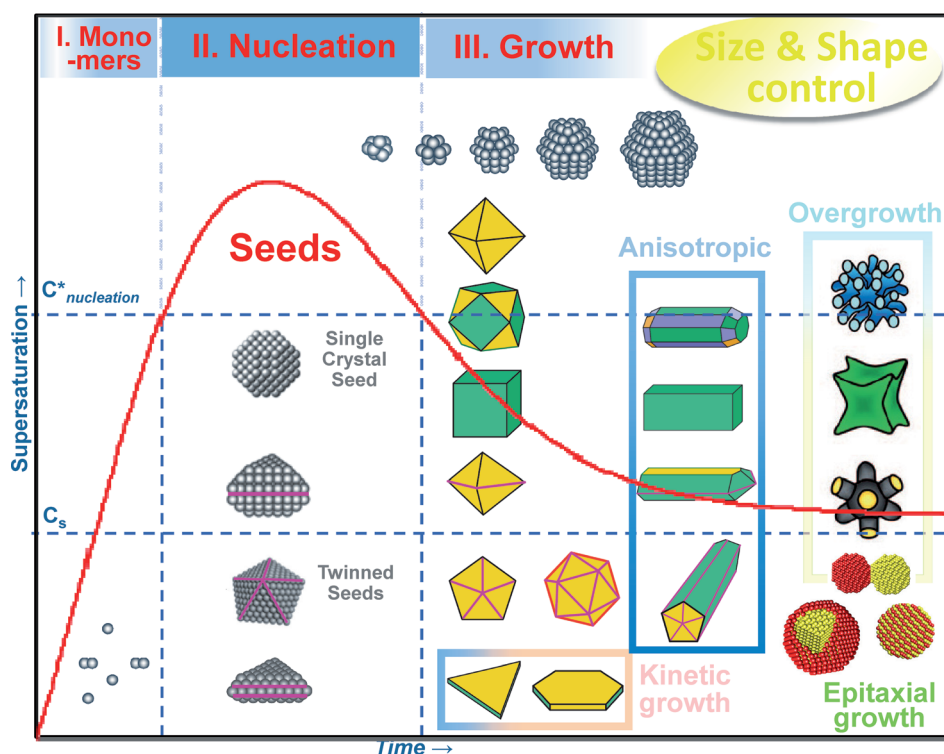


Figure 1. An illustration of general synthetic strategies for size and shape control of metal nanoparticles combining with the LaMer diagram (modified with permission from ref. [6–7], copyright 2009 and 2011 Wiley-VCH).

characterization techniques. In the last sections, we will focus on recent discoveries of the size- and shape-dependent catalytic selectivities in model catalytic studies by metal nanoparticles and the molecular factors that cause them, including structures, surface compositions, and oxidation states.

2. Colloidal Synthesis of Metal Nanoparticles

Among recent nanotechnologies, the most versatile way of fabricating metal nanoparticles with well-defined structure is the utilization of colloid chemistry. Although the most well-known and stable structure of metal nanoparticles is cubic close packing, diverse shapes can be obtained by adjusting experimental parameters by means of colloidal solution-based approaches. In the following sections, using several examples of metal nanoparticles with controlled size and shape, along with various characterization tools, we hope to provide better understanding of the specific synthetic strategies.

2.1. Understanding of colloidal synthesis of monodispersed metal nanoparticles

Four components: metal precursor, surfactant, solvent, and reducing agent are needed for the colloidal synthesis of metal nanoparticles. For a typical synthesis, desired precursors are selected and dissolved into solvent in the presence of surfactants. The reduction process then proceeds at an elevated temperature to generate metallic nanoparticles by introducing a reducing agent. Many precursors are chosen in the forms of

ionic salts, such as metal chloride, nitrate, sulfate, acetate, and, acetylacetonate. Two or more precursors can also be introduced to generate bi- or multi-metallic nanoparticles in the same batch. A surfactant endows colloidal stability of nanoparticles to prohibit aggregation and precipitation in solution.^[9] Ranging from organic molecules, to polymers, to ionic salts, many kinds of surfactants are selected, and their concentration and relative ratio to precursors dictate particle size and shape. Most of metal halides, polymers, and ammonium salt-based surfactants show good solubility in polar solvents such as water and alcohols. Surfactants play an important role in directing particle growth, and restricting particle size by interacting with metal surfaces during the reaction. As binding affinity of a surfactant varies from one crystal facet to another, a prefer-

ential binding to one certain facet results in hindering the growth of that facet which is attached to the surfactant. For this purpose, an additional surfactant as a structure-directing agent is introduced for the shape control. Clever combinations of these four general components make it possible to control the final size and shape of metal nanoparticles. Table 1 classifies basic four components for colloidal synthesis of metal nanoparticles and shows several examples. By selecting a solvent, a reaction temperature can be determined. For example, a reaction which contains metal salts in water in the presence of a polymer or an ammonium salt surfactant will proceed at 100 °C or less. In this condition, a reducing agent should be added to facilitate chemical reduction, in which metal salts with high oxidation states are reduced to zero-valent metallic nanoparticles. A polyol process is widely used to synthesize metal nanoparticles without any reducing agent, because polyalcohols such as ethylene glycol can act not only as a polar solvent but also as a reducing agent.

Typical colloidal reaction equipment consists of a stir-bar, a stir plate, a heating mantle or an oil bath, a 3-neck round bottom flask, a thermocouple, and a reflux condenser affixed to an inert gas line and bubbler.^[9] This allows for gradual and homogeneous reaction in high temperature solutions. The polyol reduction often occurs at temperatures below 200 °C, in which the polyol solvent defines the temperature and reaction rate. Some synthetic methods require a hydrothermal reactor using a stainless steel autoclave bomb to induce high pressure condition.^[10–11] To induce the reduction of a metal precursor, external energy is required as a driving force including

Table 1. Basic four components for colloidal synthesis of metal nanoparticles and their examples.

Precursors	Surfactants	Solvents	Reducing agents
<i>Ionic salts</i> (chlorides, nitrates, sulfates, acetates, acetylacetonates...)	<i>Covalent</i> · amines · carboxylic acids · thiols · phosphines <i>Electrostatic</i> · ammonium anions (CTAB, DTAB, TMAB...) Van der Waals (polymers) · PVP, PVA, PMMA, · dendrimers...	<i>Organic</i> · functional hydrocarbons (oleylamine...) <i>Polar</i> · water · alcohols (ethanol, methanol, ethylene glycol, polyethylene glycol...) <i>Non-polar</i> · hydrocarbons (<i>n</i> -hexane, toluene...) · chloroform	<i>Strong agents</i> (sodium borohydride, super hydride, lithium aluminum hydride, H ₂ gas...) <i>Weak agents</i> (hexadecanediol, acids...)

temperature, pressure, hydrothermal, microwave, and ultrasound in the solution-phase syntheses.^[12–19]

The LaMer model is widely used to explain the formation mechanism of colloidal nanoparticles.^[20–23] The three stages for the formation of nanoparticles are: super-saturation of the monomers, burst nucleation, and controlled growth toward size focusing (Figure 1). In the first stage, concentration of monomers which are formed from precursors stabilized by surfactants in solution, increases steadily as a reaction proceeds. Once the concentration of monomers reaches the critical point of supersaturation, small clusters are spontaneously generated, which causes a decrease in monomer concentration through nucleation. When the concentration of monomers drops below the critical saturation, the nucleation of new particles ceases and the available monomers are solely used for particle growth. During the nucleation period, growth may also occur simultaneously. Therefore, a short nucleation phase and slow growth kinetics should be guaranteed to minimize size broadening. Residual precursors form more stable complexes to be continuously added to existing nuclei for favorable slow growth kinetics.^[24–25]

In an alcohol reduction route, which is a popular method to synthesize metal nanoparticles, it is unclear whether the reduction process may be ahead of the birth of nuclei or not.^[6] However, both nucleation and growth kinetics can be adjusted intentionally by means of size and shape control of nanoparticles. At a given concentration of precursors in solution, the nucleation rate can be controlled by reaction temperature and time to determine the number of nuclei and remaining monomers. When preformed foreign nuclei are introduced to the precursor solution, or monomers are supplied continuously to growing nanoparticles, the formation mechanism may become versatile.^[6–7]

2.2. Size control of metal nanoparticles to the sub-nanometer scale

Significant progress has been made to synthesize metal nanoparticles based on chemical reduction process, at which a metal salt precursor is reduced in solution in the presence of a reducing agent or polyalcohol to generate zero-valent metal nanoparticles.^[6] To control the size of nanoparticles, nucleation

and growth kinetics should be governed by regulating several experimental parameters. Among them: precursor concentrations, the precursor to surfactant ratio, and a reduction temperature by choosing a solvent are all regarded as important factors. Teranishi et al. reported a method to synthesize Pt nanoparticles in the range of 1.5–5.0 nm by using chloroplatinic acid as a Pt precursor in the presence of poly-vinylpyrrolidone (PVP) in alcohols.^[26] In their report, nucleation rate was a critical factor in determining the particle size and the alcohols with a higher boiling point allowed smaller sized Pt nanoparticle. That means fewer nuclei generated by faster reduction rate at lower temperature induce a larger particle size. By decreasing the PVP to Pt⁴⁺ ratio, the resulting size of Pt nanoparticles becomes larger, owing to retarded growth by the lack of protecting groups of PVP. Through a seed-mediated growth, in which preformed nanoparticles are introduced in the precursor solution as the second step reaction, the nanoparticle size becomes larger. In the case of Pt, the final size of nanoparticles can be increased up to 10 nm.^[27] The seed-mediated growth will be dealt more in the next section as a shape control manner. The concentration of nuclei in the nucleation stage can be also regulated by the combination of two different precursors with different oxidation states. Tsung et al. synthesized Pt nanocubes with controlled sizes by introducing two Pt salts with Pt²⁺ and Pt⁴⁺ (Figure 2).^[28] When the relative ratio of Pt⁴⁺ which can be reduced much slower than Pt²⁺ in the mixture precursor was increased, the final size of nanocubes was increased by forming the fewer nuclei. Rh, Pd, Ru, and their metallic nanoparticles as well as Pt have been prepared with controlled sizes in the 1–10 nm regimes sharing the same ideas.^[29–35] Wang et al. first reported the formation of metal nanoclusters without any organic capping agent. They synthesized Pt, Rh, and Ru nanoclusters in organic media by a polyol reduction, in which both ethylene glycol and NaOH play key roles for the formation of nanoclusters and their colloidal stability.^[29] Later, this synthetic procedure is utilized to generate metal nanoparticles having different capping molecules by introducing various surfactants at the end of the reaction.^[36] Even if limited to Pt, diverse synthetic methods have been developed to synthesize monodispersed Pt nanoparticles in different media by utilizing various kinds of surfactants including PVP, oleylamine, oleic acid, ascorbic acid, trioctylphosphine, iso-

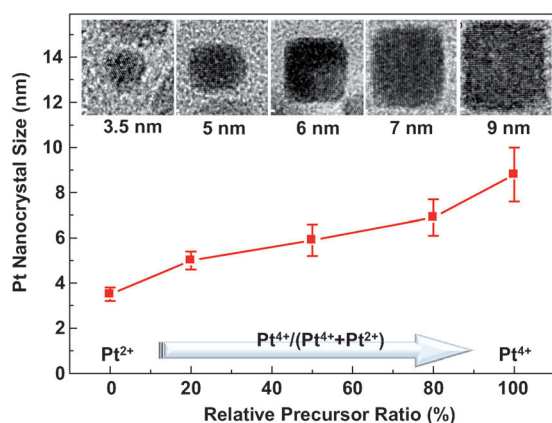


Figure 2. TEM images and sizes of Pt nanocubes as a function of relative ratio of the two precursors (modified with permission from ref. [28,94], copyright 2009 American Chemical Society).

propylacrylamide, tetradecyltrimethyl ammonium bromide, sodium polyacrylate, poly [(vinylamine)-co-(N-vinylisobutramide)], etc.^[37–43]

Nanoclusters with the particle sizes less than 1 nm, have attracted many researchers in the field of catalysis because of their extremely high surface to volume ratio.^[44] When the particle size of a metal is reduced to less than 1 nm, surface properties become dominant to show shorter nearest neighbor distances, lower melting points, and lower ionization potentials as compared to the metal in bulk. Recently, dendrimers composed of hyperbranched polymers are effectively used to prepare various metallic or bimetallic nanoparticles with size ranges less than 1 nm.^[5] The number and types of the duplicating units determine the degree of generations of dendrimers. The terminal functional groups of each branch coordinate to complexed metal species, generating metal clusters through reduction. Polyamidoamine (PAMAM) and poly(propylene imine) (PPI) are the most popular dendrimers for the synthesis of nanoclusters.^[45] For example, by varying the concentration of Pt metal ions to the PAMAM dendrimer, 0.8 and 1.0 nm sized dendrimer-encapsulated Pt nanoparticles composed of 20 and 40 Pt atoms were generated, respectively. Although the morphology of nanoclusters is hard to distinguish by using TEM, owing to their small size, a recent study shows the evolution of Pt clusters in the sub-nanometer ranges to form ordered Pt nanocrystals with polyhedral shapes in the presence of PAMAM dendrimers through high-resolution TEM.^[46] Including the dendrimer-templating strategy, recent reports have shown that now the diameter of Pt nanoparticles can be adjusted from 1 to 100 nm with narrow size distributions by using a multistep seed-mediated approach, demonstrating the infinite potential for the control of particle size.^[47]

2.3. Shape control of metal nanoparticles

The formation of metal nanoparticles can be explained by simple nucleation and growth in colloidal solution. However, there are novel strategies to affect their final shapes behind the simple growth mechanism. To understand formation of

metal nanoparticles with more complicated shapes, a nanoparticle seed formed at the last stage of nucleation, which is a cluster with well-defined structures, should be addressed. In many syntheses, shape-directing agent or additional ions, as well as the nanoparticle seeds, are also introduced to determine the final shape of metal nanoparticles.

For a fcc structure of metal nanoparticles, the most stable shape of a seed at a nucleation stage is the one with minimum surface free energy (γ), which is the energy required for creating new surface area.^[48–49] The surface energy of the fcc crystals can be evaluated that {111} surfaces are thermodynamically the most stable, owing to their lowest surface free energies, followed by {100} and then {110} surfaces. This order of surface energies of low-index faceted fcc crystals means that octahedral- or tetrahedral-shape seeds terminated with {111} facets should be favored in terms of minimizing surface energy. According to Wulff's theory, however because both octahedron and tetrahedron have larger surface areas than a cube per same volume, a truncated octahedron, so called Wulff polyhedron is the most favored shape of a single crystal seed to minimize both the surface area and interfacial free energy.^[50] This Wulff polyhedron seed has been observed in many cases of metal nanoparticle syntheses and can be grown to one of the polyhedron shapes among octahedron, cuboctahedron, and cube depending on the growth behavior during reactions.

Interestingly, singly- or multiply-twinned seeds are generated as a result of defect formation. In many cases of metal nanoparticle syntheses, a singly twinned seed is found with one twinned defect sharing a {111} mirror plane.^[51] This singly-twinned seed is enclosed by {111} and {100} facets to reduce the interfacial free energy, having a plate-like random-hcp structure. As a multiply-twinned seed, a decahedral seed, which is formed by the attachment of five single-crystal tetrahedral seeds, is commonly generated in the nucleation stage. Though each tetrahedral seed is sharing two planes with neighboring seeds to form a decahedron, a small gap will be left to have defect planes at the boundary and elongated bond lengths.^[52] Interestingly, the intrinsic properties of the singly- or multiply-twinned seeds sometimes generate elongated rods or wires as 1D structures with a later plane of either bi-pyramid or pentagon, which are in accordance with the shapes of their seeds.^[53]

The Xia group has proposed an oxidative etching to manipulate a distribution of single crystal and twinned seeds. A combination of ligand and oxygen derived from reaction solution, act as an oxidative etchant to diminish a concentration of twinned seeds selectively.^[54] By introducing trace amounts of halogen ions such as Cl^- and Br^- , or Fe-containing species, and oxygen gas to the solution, twinned seeds could be removed substantially, resulting in a high concentration of more resistant single-crystal seeds.^[6]

Since the El-Sayed group has successfully demonstrated shape controlling of Pt nanoparticles toward cube, tetrahedron, and truncated octahedron, many advances has been made regarding the role of surfactants as a shape controlling strategy of metal nanoparticles.^[55] A selection of capping agents is critical to control the shape of metal nanoparticles,

because the surface energy of crystal facets can be changed dramatically by the interactions of metal surfaces and capping agents. As one of the popular polymeric surfactants, PVP is bound strongly to the {100} facets of metal atoms. This preferential binding of the oxygen atoms of PVP to a specific surface changes the surface free energies for the crystal planes and the relative growth rates, in which {100} facets of metal atoms bound to PVP are retarded for growth, resulting in the formation of metal nanocubes by preferentially adding metal atoms to {111} facets. However, the randomly entangled polymer chains of PVP are effective in generating nanocubes with {100} terminated surfaces in a size range of more than 25 nm. In fact, several metal nanoparticles including Pt, Rh, and Ru have been synthesized in the presence of PVP through the polyol reduction to form both {100}- and {111}-terminated polyhedron shapes with a size range of less than 25 nm.^[6] In this circumstance, alkylammonium bromides such as cetyltrimethylammonium bromide (CTAB), tetradecylammonium bromide (TTAB), and dodecylammonium bromide (DTAB) show a much stronger binding affinity to the {100} surface to generate nanocubes with sizes less than 25 nm.^[28] These ionic capping agents with Br[−] as structure directing agents are widely used to synthesize various metal nanocubes with sizes < 25 nm even in the presence of PVP.^[56–57] Furthermore, specific binding of Br[−] to the {100} facets is also proven in the case of twinned-seeds to induce 1D nanostructures, in which the lateral dimensions were determined by the type of twinned-seeds such as rectangle, pentagon, octagon, and bipyramid.^[6,53]

Several additives play a crucial role to determine the shape of nanoparticles in colloidal syntheses. There are several kinds of structure directing agents including metal ions (Ag⁺, Fe³⁺, Co⁺), complexes (W(CO)₆), and reactive gas molecules (H₂, O₂, CO, NO).^[9,58–60] By introducing Ag⁺ ions, shapes of Pt nanoparticles change from cube, cuboctahedron, and octahedron as increased Ag⁺ ions (Figure 3 a–c). In a recent study, addition of Ag⁺ ions enhances a crystal growth rate along the <100> di-

rection by preferentially adsorbing on more active {100} surfaces of Pt.^[61] By controlling reduction kinetics of a polyol process and adding FeCl₃/HCl, triangular and hexagonal Pd nanoplates can be generated selectively through slow reduction (Figure 3 d–e).^[62] Anisotropic Pd nanobars bound by {100} facets can also be synthesized in the presence of KBr by broken a cubic symmetry under a kinetically controlled condition (Figure 3 f).^[63]

Seed-mediated growth is one of the well-known methods, not only to increase a crystal size, but also to control a shape of nanoparticles.^[64–65] Although the birth of a seed is already mentioned above as a means of shape control, as-made nanoparticles can be also used as a seed for the second crystal growth. During the growth, if the added metal atoms are the same component as the preformed seed, single metal nanoparticles with enhanced size and shape are generated by epitaxial growth on the surface of seeds. However, when different atoms are added to the well-faceted seed, core/shell-typed bimetallic nanoparticles can be produced. The heteroepitaxial growth occurs only at a close lattice match between the seed and the added precursors (Figure 3 g).^[7] Habas et al. prepared Pt/Pd core/shell nanocrystals by controlling the epitaxial overgrowth of a secondary metal on cubic Pt seeds.^[66–67] In this article, the shapes of Pt/Pd core/shell nanocrystals were selectively controlled from cube, to cuboctahedron, to octahedron, as NO₂ concentration was increased. As the seeded growth is combined with kinetically controlled overgrowth and selective etching, various kinds of elaborate nanostructures can be prepared such as concave cubes, multi-pods, and highly-branched dendrites.^[68–71] For instance, shapes of Pd nanoparticles can be controlled from isotropic polyhedrons under thermodynamic growth conditions to anisotropic multi-pods in kinetic regimes, in which the growth rates were controlled by relative organic surfactant ratios of oleylamine and oleic acid in a pressure reaction vessel.^[72]

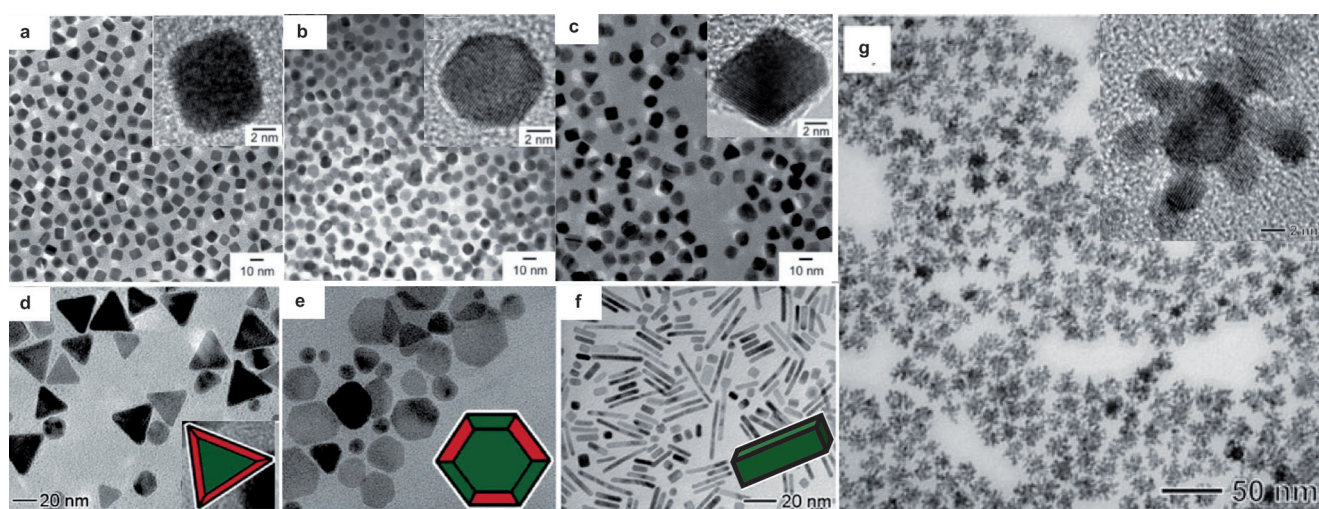


Figure 3. TEM and high-resolution TEM (insets) images of shape controlled nanoparticles: a) Pt cubes, b) Pt cuboctahedra, c) Pt octahedra, d) Pd triangular plates, e) Pd hexagonal plates, f) Pd nanobars, and g) Pd–Pt bimetallic nanodendrites (modified with permission from ref. [61–63]), copyright American Chemical Society and ref. [68], 2009 copyright American Association for the Advancement of Science).

3. Nanoparticle-based Catalysts

3.1. Nanoparticle-based catalysts and mesoporous materials

Single-crystalline metals, grown to expose specific surfaces, have been widely used for modeling industrial catalysts, owing to their lack of complexity and the ability to work with a clean surface.^[73–74] Recent developments in colloidal chemistry facilitate the extension of model studies of catalysis from single-crystal metal surfaces to nanoparticles.^[74] To use nanoparticles as a heterogeneous catalyst, as-synthesized metal nanoparticles should be placed either on a 2D substrate or into an oxide support (Figure 4a). Conventionally 2D catalysts are fabricated by self-assembled nanoparticles as a monolayer deposited on

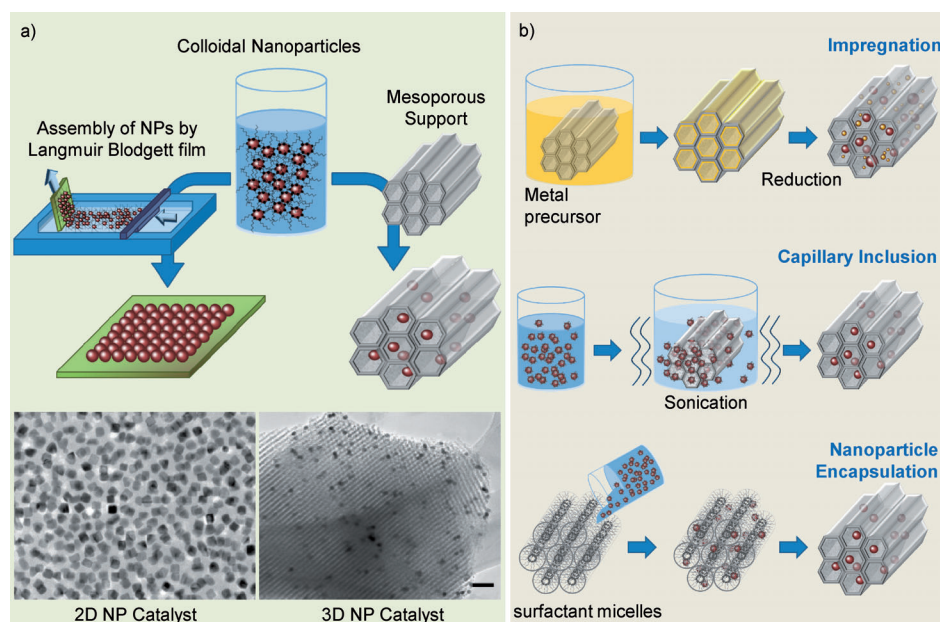


Figure 4. a) The design of colloidal nanoparticle-based catalysts and b) preparation strategies for 3D catalysts supported on mesoporous materials.

a substrate through the Langmuir–Blodgett technique. After deposition, the organic capping molecules can be removed by UV/ozone treatment to endow a clean surface of nanoparticles.^[75] For 3D catalysts, metal nanoparticles are incorporated into high-surface area mesoporous oxides as a support. The mesoporous silica materials such as SBA-15 and MCF-17 have been utilized widely as a support, owing to their high surface area, ordered channel structure, and large pore volume.^[76] Current industrial catalysts are prepared through impregnation methods, in which metal salts precipitated out of solution onto an oxide and thermally reduced to form nanoparticles. However, the prepared catalysts have a broad size distribution of nanoparticles, because thermal activation and reduction are very difficult to control during the nanoparticle formation. Two approaches are developed to prepare for 3D catalysts with a controlled size of nanoparticles: capillary inclusion and nanoparticle encapsulation (Figure 4b).^[9] Colloidal nanoparticles can be loaded into mesoporous materials by the

capillary induced inclusion, in which the sonication promotes homogeneous dispersion of nanoparticles thorough the entire channel. Recently, the nanoparticle encapsulation method was developed for the direct encapsulation of pre-made metal nanoparticles into a supporting silica matrix during the hydrothermal growth of mesoporous silica.^[77] Now, 2D and 3D nanoparticle-based catalysts can be a bridge between single crystals and industrial catalysts for model catalytic studies. To determine active surface sites of nanoparticle-based catalysts, ethylene hydrogenation is chosen as a probe reaction. The exothermic ethylene hydrogenation as a representative structure insensitive reaction turns over to produce ethane over 10 times per metal surface site per second at room temperature on Pt surface.^[78]

Beyond the most-investigated silica materials, mesoporous oxides have attracted much interest as a support because oxide-metal interfaces affect catalytic activity and selectivity. Several mesoporous oxides such as γ -alumina (γ -Al₂O₃), TiO₂, Nb₂O₅, and CeO₂ are chosen and utilized as an excellent support, owing to its acid/base properties for many catalytic reactions.^[79–80] There are two different pathways to prepare ordered mesoporous oxides: soft-templating (cooperative assembly) and hard-templating (nanocasting) approaches.^[81–82] Through the cooperative assembly of inorganic metal precursors and organic surfactants as a soft template, mesoporous oxides can be directly synthesized by a simple sol-gel process.^[76] However, this approach is limited to several

metal oxides, owing to poor phase separation during framework crystallization and subsequent loss of mesostructure. The hard-templating approach provides efficient and versatile ways to synthesize crystalline mesoporous materials with controlled pore structures, because the hard templates determine the final structure and make them stable during high-temperature crystallization.^[83]

3.2. Characterization of nanoparticle-based catalysts

Since the first commercial electron microscope was installed by I. G. Farben-Werke in 1939, transmission electron microscopy (TEM) has been developed to characterize nanostructural materials. With the development of TEM and its associated techniques, the renaissance of the nanotechnology has been experienced in the new century. Nowadays, TEM provides not only high-resolution lattice images, but also chemical identification of single nanoparticles at an atomic scale.^[84] Crystal

structures of nanoparticles can be identified by electron, neutron, and X-ray diffraction. The development of colloidal chemistry allows design elaborated nanostructures including bi- or multi-metallic, core/shell or multi-shelled, highly-branched, and hollow materials. Recently highly-branched bimetallic Pd–Pt nanodendrites made by means of the epitaxial overgrowth method, were observed by using high-resolution TEM, to contain Pt branches distributed over the entire surface of the Pd nanoparticle core (Figure 3 g).^[68] Electron energy-loss spectroscopy (EELS) and energy dispersive X-ray (EDS) mapping, combining scanning transmission electron microscopy (STEM), have become more attractive to analyze the chemical composition of unprecedented nanostructures. Figure 5a–b show a high angle annular dark field (HAADF) image of CuNi bimetallic nanoparticles and the corresponding line scan profile in STEM using energy dispersive X-ray (EDS) spectra, suggesting the bimetallic nanoparticles are composed of a Cu-rich core and a Ni-rich shell (Figure 5a–b).^[85] Apart from the commonly used characterization tools, in situ characterization techniques have been developed to enable real-time monitoring of atomic structures during chemical synthesis and to identify surface structure, composition, and oxidation states of nanoparticles under catalytic reaction conditions. Such techniques in situ include: environmental TEM, time-resolved XRD, synchrotron-based X-ray photoelectron, near-edge X-ray absorption fine structure (NEXAFS) spectroscopy, high pressure scanning tunneling microscopy (HPSTM), and ambient pressure X-ray photoelectron spectroscopy (APXPS) (See Table 2).^[86] The Alivisatos group demonstrated that Pt nanoparticles can grow either by monomer attachment from solution or by particle coalescence by using in situ TEM which was designed to observe the dynamic growth of nanoparticles in solution.^[87] Recently, the Tilley group also conducted in situ studies on the growth and shape evolution of Pt

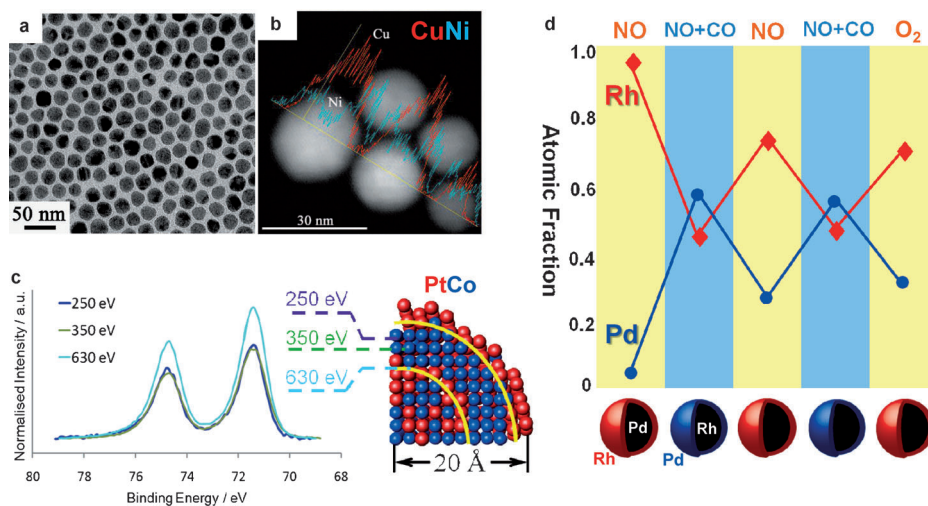


Figure 5. a) TEM, and b) HAADF-STEM images of CuNi bimetallic nanoparticles and their X-ray line scan profile of energy dispersive spectroscopy (EDS) along the line. c) Ambient pressure Pt 4f XP Spectra of PtCo bimetallic nanoparticles in the presence of H₂ at 3 different photon energies. Schematic model corresponding to a 7-layer nanoparticle containing the ratios of Co (blue) and Pt (red) atoms present in each region, demonstrating that Pt was segregated to the surface under H₂ atmosphere. d) Relative atomic fractions of Rh (red) and Pd (blue) in RhPd bimetallic nanoparticles as measured by APXPS under oxidizing (0.1 torr of NO or O₂) and catalytic reaction (0.1 torr NO mixed with 0.1 torr CO) conditions, demonstrating reversible changes of the surface compositions under the reaction conditions (modified with permission from ref. [85], copyright 2008 American Chemical Society, ref. [90], copyright 2011 Springer, and ref. [91], copyright 2008 American Association for the Advancement of Science).

Table 2. Commonly used ex situ and in situ techniques for characterizations of nanoparticles.

Characterization Techniques	
Ex situ characterization	Transmission Electron Microscopy (TEM) Energy-Dispersive X-ray (EDX) Analysis Scanning Electron Microscopy (SEM) Atomic Force Microscopy (AFM) X-ray Diffraction (XRD) Small-Angle X-ray Scattering (SAXS) X-ray Photoelectron Spectroscopy (XPS) Physisorption and Chemisorption by Brunauer–Emmett–Teller (BET) Analysis UV/Vis spectroscopy Thermogravimetric Analysis (TGA) Inductively Coupled Plasma—Optical Emission Spectroscopy (ICP-OES)
In situ characterization	Environmental Transmission Electron Microscopy (TEM) Electron Energy-Loss Spectroscopy (EELS) Time-resolved X-ray Diffraction (XRD) Diffuse Reflectance Infrared Fourier-Transform Spectroscopy (DRIFTS) High-Pressure Scanning Tunneling Microscopy (HPSTM) Sum Frequency Generation Vibrational Spectroscopy (SFGVS) Ambient-Pressure X-ray Photoelectron Spectroscopy (APXPS) UV-Raman and Surface Enhanced Raman Spectroscopy (SERS) Near-Edge X-ray Absorption Fine Structure (NEXAFS)

nanoparticles in solution by using synchrotron-based XRD technique.^[88] In their report, the growth of Pt nanoparticles in the low-concentration reaction occurred at a relatively slow rate in the thermodynamic controlled regime to generate faceted particles. On the contrary, the high concentration reaction generated Pt nanoparticles with highly branched structures by the fast growth rate under the kinetically controlled regime. An increased demand of in situ techniques, is the understanding of nanoparticles at an atomic scale under reaction environ-

ments of pressure and temperature, that are encountered during conventional catalytic reactions.^[89] Recently, CO₂ hydrogenation as an analogue of the Fischer–Tropsch reaction was conducted over CoPt bimetallic nanoparticles.^[90] In this study, in situ NEXAFS results showed that Co remained fully reduced during the reaction in the presence of Pt, however XPS and TEM data collected during exposure to a reducing hydrogen atmosphere revealed that Pt segregates to the surface during the reaction, preventing the access of reactants to the cobalt as a main catalyst (Figure 5c). Similarly, bimetallic RhPd nanoparticles underwent reversible compositional changes under different catalytic conditions of oxidizing (with NO or O₂) and reducing (NO and CO) atmospheres.^[91] In Figure 5d, HPXPS results clearly show that, Rh atoms were pulled to the surface during oxidizing conditions and reversibly went back to the core when changed to the reducing conditions. The authors attributed this transformation to the fact that Pd has a lower surface energy than Rh therefore it tends to migrate to the surface when reduced.

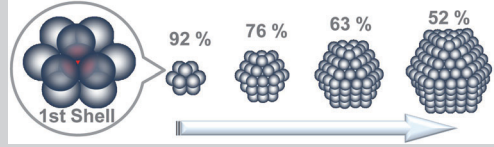
4. Reaction Selectivities by Nanoparticles

The ultimate goal of a catalyst in the 21st century is to actualize green chemistry, achieving 100% selectivity of the desired product molecule in multipath reactions.^[92] To get only one desired product molecule out of many thermodynamically stable molecules is a very challenging undertaking. However, it is believed that only nanoparticles with well-defined structures offer a solution. This is because the major product in catalytic conversion is determined by the unique atomic structure of a metal surface. Although, many studies demonstrate that catalytic activity can be enhanced from nanoparticle sizes, owing to their high surface area and surface roughness, few studies have shown changes in product selectivity. In this chapter, several multipath reactions will be introduced to demonstrate structure-dependent catalytic selectivity.

4.1. Size-dependent selectivity

As well as catalytic activity, dramatic changes of selectivity occur in metal nanoparticles in the size regimes of 1–10 nm, which are identical to the size of heterogeneous metal catalysts used as industrial catalysts. Considering the surface to volume ratio of a nanocrystal, we can easily estimate the percentage of surface atoms of metal nanoparticles as a function of size. A metal atom can be surrounded by 12 atoms to become the completely shelled cluster with 13 atoms. To have n shelled atoms in an fcc structure, $10n^2 + 2$ atoms are needed for each shell, while $2n + 1$ atoms on a sectional plane become a diameter of a crystal.^[44] From Table 3, Pt with an atomic diameter of 0.27 nm, has 92% surface atoms when it becomes a particle with a diameter of 0.8 nm by adding one outer shell, then the surface ratios are abruptly decreased to 45 and 35% for the diameters of ca. 3 and 4 nm, respectively. From these calculations, there is nothing intrinsically unusual that catalytic reactions undergo dramatic changes in the sizes of less than 5 nm in terms of the surface area per a given size.

Table 3. Calculated sizes of Pt nanoparticles and corresponding surface atom percentages, assuming that nanoparticles are formed as a completely shelled polyhedron.



# of shells (n)	# of atoms in n th shell (=10n ² +2)	Total # of atoms	# of atom on a diameter (=2n+1)	Surface atoms [%]	Size of Pt NPs [nm]
0		1	1	–	0.3
1	12	13	3	92	0.8
2	42	55	5	76	1.4
3	92	147	7	63	1.9
4	162	309	9	52	2.4
5	252	561	11	45	3.0
6	362	923	13	39	3.5
7	492	1415	15	35	4.1
8	642	2057	17	31	4.6
9	812	2869	19	28	5.1

From tremendous catalytic studies on bulk single-crystalline surfaces under ultra-high vacuum (UHV) conditions, it is well known that the specific crystallographic plane has great influence on catalytic pathways and activities. For a last decade, the Somorjai group has been studying the effect of nanoparticle size for several multipath hydrogenation reactions with furan, crotonaldehyde, pyrrole, benzene, and methylcyclopentane.^[8] Surface sum frequency generation vibrational spectroscopy (SFGVS) is an in situ surface characterization technique that was developed to study surface-related phenomena in reaction conditions. Through this technique, surface structures regarding adsorbate configuration and orientation on metal surfaces can be confirmed, and reaction intermediates and spectator molecules are discovered. This technique plays a key role to bridge the material gap between model single crystal surfaces and self-assembled monolayers of nanoparticles contributing to the understanding of dynamic surface phenomena.

Furan is a five-membered aromatic ring, in which one of the two lone paired electrons is delocalized over the ring. Upon hydrogenation reactions, furan is reduced to form dihydrofuran (DHF), tetrahydrofuran (THF), or cracked to butanol and propylene by ring opening (Figure 6a). In furan hydrogenation over Pt nanoparticles at 90 °C, the higher selectivity of ring-opening toward butanol was shown for larger nanoparticles which is also confirmed on {100} facets of Pt single crystal surfaces.^[93] On the contrary, small particles preferentially yielded dihydrofuran by a partial hydrogenation of the aromatic ring. Butanol formed over 7 nm Pt nanoparticles only at lower temperatures, but vanished as temperature increased, however it was not observed over the 1 nm particles at any temperatures. The same trends were confirmed from SFGVS studies on Pt {111}, namely that the planar furan ring lies parallel to the metal surface. In SFGVS spectra, the concentration of butoxy intermediate increases with increasing temperature on the Pt

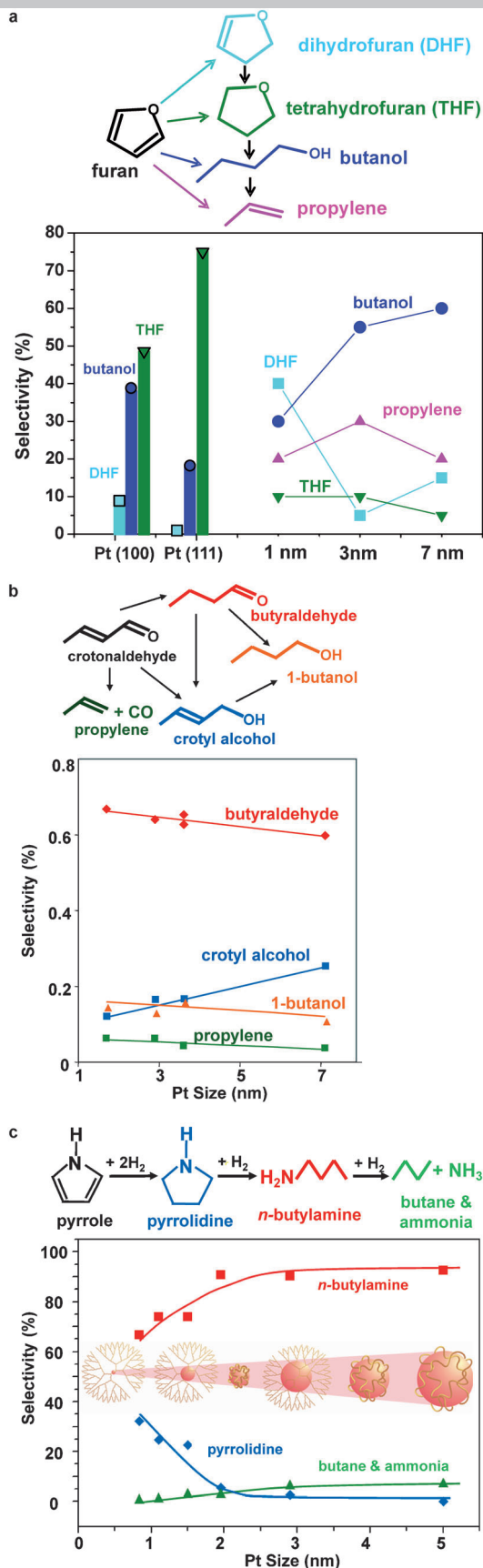


Figure 6. Dependence of selectivity as a function of Pt nanoparticle size in multipath hydrogenation reactions: a) furan, b) crotonaldehyde, and c) pyrrole (modified with permission from ref. [93–97], copyright 2008–2010 American Chemical Society).

(111) surface, and THF is found in an upright binding geometry to the surface, which is in accordance with reaction data over Pt (111) from THF toward butanol as temperature is increased. The SFGVS spectra also indicates a parallel furan adsorption over Pt(100) under hydrogenation conditions and confirms both butanol and THF are seen bound to the Pt(100) surface in upright geometries. The structural information of these reaction preferences were also investigated using SFGVS over Pt nanoparticles.^[94] In Figure 7, a parallel furan adsorption

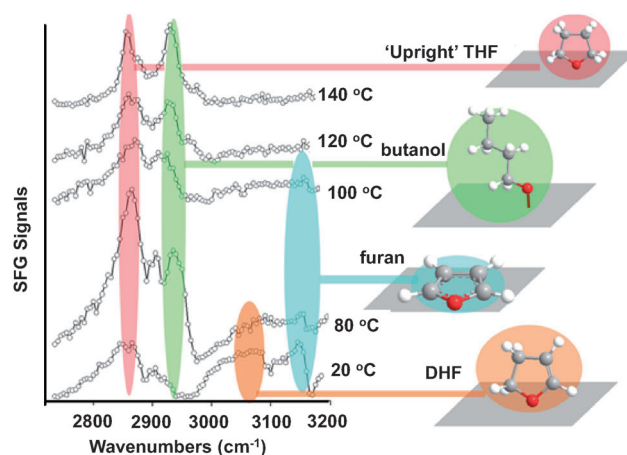


Figure 7. Sum frequency generation vibrational spectroscopy (SFGVS) spectra in the methyl region obtained under the furan hydrogenation reaction (10 torr furan, 100 torr H₂, and balance He) over 1 nm sized Pt nanoparticles in the temperature from 20 to 140 °C (modified with permission from ref. [9], copyright 2012 Elsevier and ref. [93], copyright 2010 American Chemical Society).

on the surface of 1 nm sized Pt nanoparticles was shown in the SFG spectrum below 100 °C. Above 100 °C, butoxy adsorbates bonded thorough their oxygen atoms to the surface in an upright binding geometry with upright THF, whereas decreased dihydrofuran was observed. Interestingly, 1–7 nm Pt nanoparticles exhibited a tendency toward further cracking products to form propylene in the reaction.

The hydrogenation of α,β -unsaturated aldehydes is of interest to serve as a useful probe of catalytic chemoselectivity due to their two different types of double bonds (C=C and C=O). Crotonaldehyde can be chosen for the purpose of an interesting selectivity study toward industrially desired unsaturated alcohols. Size dependence of crotonaldehyde hydrogenation was studied on Pt nanoparticles supported on mesoporous silica SBA-15 (Figure 6b). In Figure 6b, as increased particle sizes from 1.7 to 7.1 nm, the selectivity towards crotyl alcohol in 8 torr crotonaldehyde (1 torr = 0.133 kPa), 160 torr H₂ at 80 °C.^[95–96] The decarbonylation to form propylene and CO is preferred over smaller nanoparticles due to increased deactivation, which is confirmed in CO poisoning experiments.

Pyrrole hydrogenation was conducted over Pt nanoparticles supported on SBA-15 with the size range of 0.8–5.0 nm, in which size variations can be achieved by selective choices of capping agents: PAMAM dendrimer and PVP (Figure 6c).^[97] As the particle size decreased below 2 nm, unique selectivity was

led toward formation of pyrrolidine, while ring opening to *n*-butylamine was retarded. That is also in accordance with furan hydrogenation that the smaller nanoparticles preferentially yield the partially saturated ring. It is speculated that the nitrogen of *n*-butylamine is much more electron-rich than pyrrolidine and pyrrole, so it will form strong adsorbate-surface interactions which become stronger over smaller nanoparticles. Although the surface to volume ratio is increased substantially when using reduced particle sizes, as described above, we must also consider the oxidation states of Pt nanoparticles. In the previous studies on the synthesis of Pt and Rh nanoclusters encapsulated by 4th generation PAMAM dendrimers, XPS measurements of 20 atoms of Pt and 30 atoms of Rh show that about 93% of the Pt and 44% of Rh are oxidized.^[45] It was speculated that the size and oxidation state of nanoparticles directly influence their catalytic selectivity, these effects are greatly enhanced as the size is decreased to about 1 nm and below. A similar observation of oxide shell was found on Rh nanoparticles synthesized with sizes of 2–12 nm. In the studies of CO oxidation, turnover rates on the 2 nm Rh nanoparticles were 8 times higher than those of the 12 nm. It was also demonstrated by the strong peaks in APXPS corresponding to rhodium oxides for the 2 nm nanoparticles.^[98] Partially oxidized metal nanoparticles induced an interface between the oxide surface and metallic core, and thus the presence of interfaces, combined with the strain generated by their small size, make them less stable and more reactive in reactions.

Very recently, our group also demonstrated size dependent selectivities of hydrogenative reforming reactions of *n*-hexane over Pt and other bimetallic nanoparticles as a function of size and composition. Uniformly synthesized metallic and bimetallic nanoparticles with controlled sizes facilitate study of many fundamental and industrially useful catalytic reactions.

4.2. Shape-dependent selectivity

To date, one of the representative examples of shape dependent selectivity is benzene hydrogenation over Pt nanoparticles with shapes of cube and cuboctahedron.^[99] Pt-catalyzed hydrogenation of benzene with single-crystalline Pt surfaces produces two molecules, cyclohexane and cyclohexene, on the platinum (111) surface, while cyclohexene is the sole molecule produced on the (100) surface (Figure 8a). This dependence on Pt single crystals can be extended and compared to nanoparticles with well-defined surfaces. It has been shown that

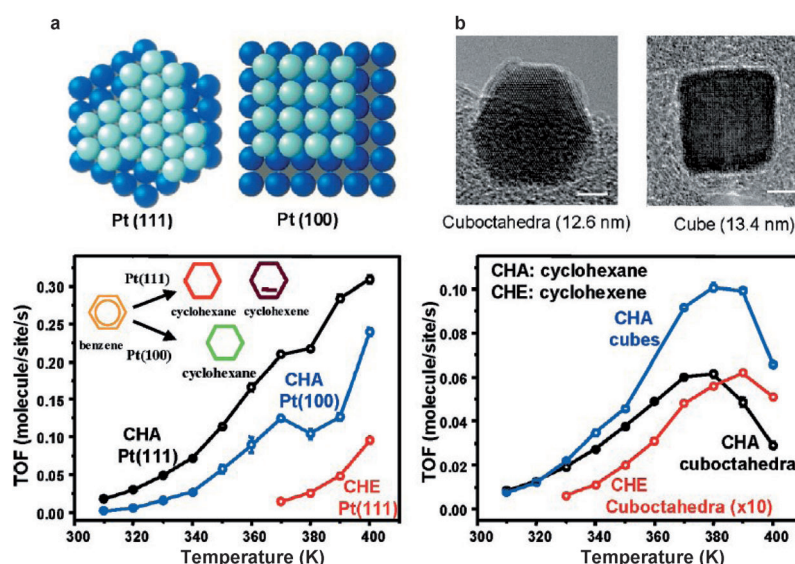


Figure 8. Turnover rates of the benzene hydrogenation reaction on a) Pt (111) and (100) single crystalline surfaces compared with on b) Pt nanoparticles with the shapes of cuboctahedron and cube (modified with permission from ref. [94,99], copyright 2007 and 2009 American Chemical Society).

a similar trend was observed on nanoparticle arrays of cubic and cuboctahedral Pt nanoparticles (Figure 8b). Although cuboctahedral Pt nanoparticles with (100) facets give rise to two products, Pt cubes generate only benzene, which is in accordance to the single crystal studies.

The other example of shape dependent selectivity on Pt surfaces has been shown in olefin conversions between its *cis*- and *trans*-isomers, again allowing a bridging of the materials gap between single-crystal surfaces and nanoparticles (Figure 9). In food chemistry, the selective production of *cis* olefins is much desirable because *trans* fats have been linked

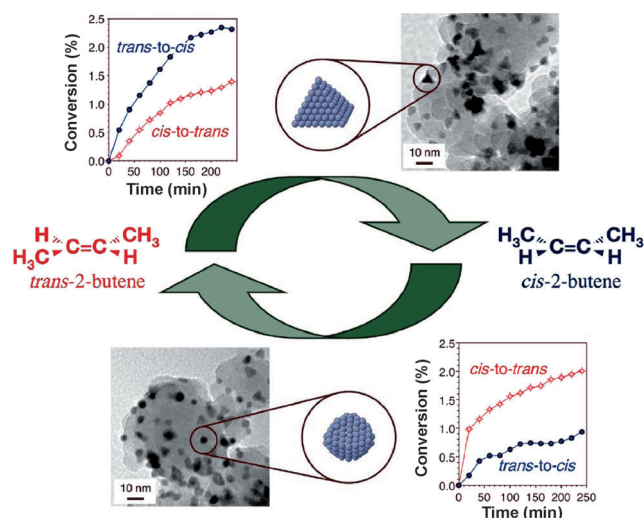


Figure 9. Catalytic selectivity during alkene *cis-trans* isomerization reactions as a function of Pt nanoparticle shape and corresponding TEM images: (111) faceted tetrahedral Pt nanoparticles yield the *cis* isomer preferentially, whereas spherical Pt nanoparticles form the *trans* isomer (modified with permission from ref. [102], copyright 2009 American Chemical Society).

to serious health effects. Thus, it is of crucial importance to suppress the production of undesirable but thermodynamically stable *trans* isomers. The Zaera group had already shown that the (111) facet of Pt favors *cis* olefins production in their model Pt single-crystal studies.^[100–102] Later they drew identical results from shaped nanoparticles that tetrahedral Pt nanoparticles with (111) facets supported onto a silica promoted much preferential conversion of *trans*-2-buten to *cis*-2-butane than those of either cubic or spherical nanoparticles using 10 torr butane and 0.2 torr H₂ at 100 °C.

Recent studies on methylcyclopentane (MCP) hydrogenolysis reactions using 10 torr MCP and 50 torr H₂ at 160–300 °C over Pt nanoparticles demonstrates distinct selectivity depending on the particle shape.^[103] The hydrogenolysis of MCP yields various C₆ isomers through ring opening and a subsequent isomerization, and benzene through ring-enlargement and dehydrogenation, and cracking products (Figure 10). Although the reaction proceeds dominantly on the (110) facet of Pt octahedra and high indexed spheres, hexane was a major product on octahedral, whereas spheres led to 2-methylpentane at 240 °C. On Pt cubes (100) cracked C₁–C₅ products were maximized through C–C bond breakage. At elevated temperatures, formation of benzene is much preferred by ring closure of C₆ isomers and subsequent dehydrogenation which is dominated on (100) faceted Pt cubes and (100) and (111) faceted cubocta-

hedra. In this study, shapes of Pt nanoparticles and reaction temperatures affect strongly to both activity and selectivity, owing to different surface crystallographic orientations.

For multipath reactions, there are small energy differences among several reaction products with different potential energy barriers, compared to a single reaction with relatively high activation energy to yield only one product. Product selectivity is determined by the relative energy differences among the activation energies of possible products. Small differences in competing potential energy barriers can cause dramatic changes in product selectivity.^[102] Several molecular factors affect product selectivity in catalysis. Recent reaction studies combined with in situ characterization techniques have identified that surface structures, compositions, and oxidation states of metals, characteristic mobility or restructuring of adsorbates, reaction intermediates, and charge transfer during catalysis are the main factors which affect reaction selectivity.^[8] With metal nanoparticles, it is a proven factor that the catalytic selectivity during multipath reactions strongly depends on the surface natures of the nanoparticles.

5. Conclusions and Outlook

Selectivity is of key importance to heterogeneous catalysis in 21st century and is achievable by nanoparticle-based catalysts as their surface structures and active sites are tailored at the molecular level. New tools based on colloidal chemistry have been developed to control uniformity, size, shape, composition, and functionality of metal nanoparticles. In this perspective, we have suggested several multipath reaction studies to ascertain how the size and shape of nanoparticles can contribute to selectivity in the field of catalysis. However, the catalytic mechanisms of real catalysts and the surface complexity of nanoparticles still remain a challenging task. One of the major challenges in catalysis is the removal of surface capping molecules. The surfactant for nanoparticle synthesis plays a key role in endowing colloidal stability and surface regulations determining the particle morphology. Recent reports show that among various capping molecules, polymeric surfactants such as PVP stabilizing the surface of Pt nanoparticles turn out to act much less as a catalytic poison than other ionic or amine surfactants.^[36] Although thermal oxidation or UV/ozone treatment has been used effectively to remove capping agents, the clean surface of metal nanoparticles and the effect of remaining surfactants during reactions are still debated issues. Furthermore, the stability of nanoparticles in high temperature reactions against agglomerations or surface smoothing should be overcome not to lose the surface structures of nanoparticles. Recently, core/shell-type Pt nanoparticles with mesoporous silica shells have been developed as a thermally stable catalyst, however, pore size, thickness of the shells, kinds of shell materials, and their large-scale production should be developed for diverse and effective applications.^[104]

One of major advances of nanoparticle catalysts is building a bridge between homogeneous and heterogeneous catalyst. Dendrimer-encapsulated metal nanoclusters with the size of 1 nm or less, which is the fruit of the most advanced size

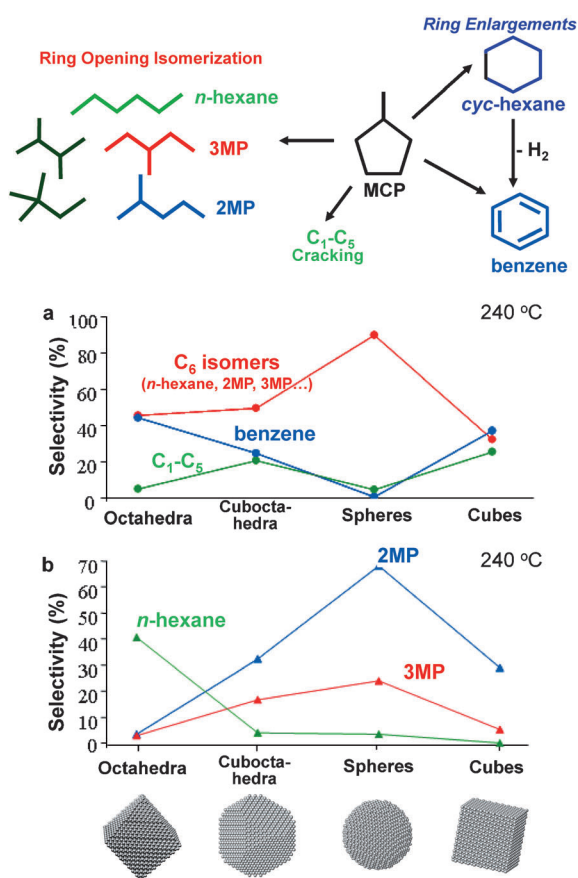


Figure 10. Dependence of the selectivity as a function of Pt nanoparticle shape in the methylcyclopentane (MCP) hydrogenolysis reaction (modified with permission from ref. [103], copyright 2011 Springer).

ranges accomplished by a colloidal technique, show similar and sometimes even higher turnover rates than those of homogeneous catalysts.^[105] Also, studies on metals covered with an oxide provide the evidence of hot electron generation at metal surfaces during exothermic reactions, which have led to the fabrication of a catalytic nanodiode, where metals are deposited on an oxide to form a Schottky barrier.^[106] Many catalytic reactions with metals contacted with oxides show great promise of a strong metal support interaction at the oxide-metal interface.^[107] The great advances of nanotechnology can not only lead to a new way for the design of ideal catalysts achieving near 100% product selectivity at maximum activity but also open new possibilities for multidisciplinary research among catalysis, electronics, biology, environment, and energy.

Acknowledgements

This work was funded by the Director, Office of Science, Office of Basic Energy Sciences, and the U.S. Department of Energy under Contract No DE-AC02-05CH11231. The nanoparticle synthesis was partially funded by Chevron Corp. We thank Nathan Musselwhite for valuable discussion.

Keywords: catalyst • colloid • in situ characterization • nanoparticles • selectivity

- [1] G. Schmid, *Nanoparticles: From Theory to Application*, Wiley-VCH, Weinheim, **2004**.
- [2] K. J. Klabunde, *Nanoscale Materials in Chemistry*, Wiley, New York, **2001**.
- [3] G. Ertl, H. Knözinger, J. Weitkamp, *Handbook of Heterogeneous Catalysis*, Wiley-VCH, Weinheim, **1997**.
- [4] G. A. Somorjai, *Introduction to Surface Chemistry and Catalysis*, Wiley, **1994**.
- [5] E. gross, J. Krier, L. Heinke, G. A. Somorjai, *Top. Catal.* **2012**, *55*, 13–23.
- [6] Y. N. Xia, Y. J. Xiong, B. Lim, S. E. Skrabalak, *Angew. Chem.* **2009**, *121*, 62–108; *Angew. Chem. Int. Ed.* **2009**, *48*, 60–103.
- [7] B. Lim, Y. N. Xia, *Angew. Chem.* **2011**, *123*, 78–87; *Angew. Chem. Int. Ed.* **2011**, *50*, 76–85.
- [8] G. A. Somorjai, J. Y. Park, *Angew. Chem.* **2008**, *120*, 9352–9368; *Angew. Chem. Int. Ed.* **2008**, *47*, 9212–9228.
- [9] K. An, S. Alayoglu, T. Ewers, G. A. Somorjai, *J. Colloid Interface Sci.* **2012**, *373*, 1–13.
- [10] X. Wang, J. Zhuang, Q. Peng, Y. D. Li, *Nature* **2005**, *437*, 121–124.
- [11] Z. Q. Niu, Q. Peng, M. Gong, H. P. Rong, Y. D. Li, *Angew. Chem.* **2011**, *123*, 6439–6443; *Angew. Chem. Int. Ed.* **2011**, *50*, 6315–6319.
- [12] F. Gao, Q. Y. Lu, S. Komarneni, *Chem. Mater.* **2005**, *17*, 856–860.
- [13] V. Abdelsayed, A. Aljarash, M. S. El-Shall, Z. A. Al Othman, A. H. Alghamdi, *Chem. Mater.* **2009**, *21*, 2825–2834.
- [14] J. A. Gerbec, D. Magana, A. Washington, G. F. Strouse, *J. Am. Chem. Soc.* **2005**, *127*, 15791–15800.
- [15] J. T. Ren, R. D. Tilley, *J. Am. Chem. Soc.* **2007**, *129*, 3287–3291.
- [16] J. Ren, R. D. Tilley, *Small* **2007**, *3*, 1508–1512.
- [17] K. S. Suslick, M. M. Fang, T. Hyeon, *J. Am. Chem. Soc.* **1996**, *118*, 11960–11961.
- [18] X. Wang, Y. D. Li, *Chem. Commun.* **2007**, 2901–2910.
- [19] Y. J. Song, J. Hormes, C. S. S. R. Kumar, *Small* **2008**, *4*, 698–711.
- [20] G. P. Ford, V. K. Lamer, *J. Am. Chem. Soc.* **1950**, *72*, 1959–1964.
- [21] V. K. Lamer, R. H. Dinegar, *J. Am. Chem. Soc.* **1950**, *72*, 4847–4854.
- [22] T. Sugimoto, *Monodispersed Particles*, Elsevier, Amsterdam, **2001**.
- [23] T. Sugimoto, *Adv. Colloid Interface* **1987**, *28*, 65–108.
- [24] S. G. Kwon, T. Hyeon, *Acc. Chem. Res.* **2008**, *41*, 1696–1709.
- [25] J. Park, J. Joo, S. G. Kwon, Y. Jang, T. Hyeon, *Angew. Chem.* **2007**, *119*, 4714–4745; *Angew. Chem. Int. Ed.* **2007**, *46*, 4630–4660.
- [26] T. Teranishi, M. Hosoe, T. Tanaka, M. Miyake, *J. Phys. Chem. B* **1999**, *103*, 3818–3827.
- [27] R. M. Rioux, H. Song, J. D. Hoefelmeyer, P. Yang, G. A. Somorjai, *J. Phys. Chem. B* **2005**, *109*, 2192–2202.
- [28] C. K. Tsung, J. N. Kuhn, W. Y. Huang, C. Aliaga, L. I. Hung, G. A. Somorjai, P. D. Yang, *J. Am. Chem. Soc.* **2009**, *131*, 5816–5822.
- [29] Y. Wang, J. W. Ren, K. Deng, L. L. Gui, Y. Q. Tang, *Chem. Mater.* **2000**, *12*, 1622–1627.
- [30] Y. W. Zhang, M. E. Grass, S. E. Habas, F. Tao, T. F. Zhang, P. D. Yang, G. A. Somorjai, *J. Phys. Chem. C* **2007**, *111*, 12243–12253.
- [31] S. M. Humphrey, M. E. Grass, S. E. Habas, K. Niesz, G. A. Somorjai, T. D. Tilley, *Nano Lett.* **2007**, *7*, 785–790.
- [32] T. Teranishi, M. Miyake, *Chem. Mater.* **1998**, *10*, 594–600.
- [33] G. Viau, R. Brayner, L. Poul, N. Chakroune, E. Lacaze, F. Fievet-Vincent, F. Fievet, *Chem. Mater.* **2003**, *15*, 486–494.
- [34] S. H. Joo, J. Y. Park, J. R. Renzas, D. R. Butcher, W. Y. Huang, G. A. Somorjai, *Nano Lett.* **2010**, *10*, 2709–2713.
- [35] C. A. Stowell, B. A. Korgel, *Nano Lett.* **2005**, *5*, 1203–1207.
- [36] J. N. Kuhn, C. K. Tsung, W. Huang, G. A. Somorjai, *J. Catal.* **2009**, *265*, 209–215.
- [37] C. Wang, H. Daimon, T. Onodera, T. Koda, S. H. Sun, *Angew. Chem.* **2008**, *120*, 3644–3647; *Angew. Chem. Int. Ed.* **2008**, *47*, 3588–3591.
- [38] L. Wang, Y. Yamauchi, *J. Am. Chem. Soc.* **2009**, *131*, 9152–9153.
- [39] C. W. Chen, M. Akashi, *Langmuir* **1997**, *13*, 6465–6472.
- [40] Y. J. Song, Y. Yang, C. J. Medforth, E. Pereira, A. K. Singh, H. F. Xu, Y. B. Jiang, C. J. Brinker, F. van Swol, J. A. Shelnutt, *J. Am. Chem. Soc.* **2004**, *126*, 635–645.
- [41] S. W. Kim, J. Park, Y. Jang, Y. Chung, S. Hwang, T. Hyeon, Y. W. Kim, *Nano Lett.* **2003**, *3*, 1289–1291.
- [42] S. W. Chen, K. Huang, J. A. Stearns, *Chem. Mater.* **2000**, *12*, 540–547.
- [43] J. Y. Chen, B. Lim, E. P. Lee, Y. N. Xia, *Nano Today* **2009**, *4*, 81–95.
- [44] J. P. Wilcoxon, B. L. Abrams, *Chem. Soc. Rev.* **2006**, *35*, 1162–1194.
- [45] W. Huang, J. N. Kuhn, C. K. Tsung, Y. Zhang, S. E. Habas, P. Yang, G. A. Somorjai, *Nano Lett.* **2008**, *8*, 2027–2034.
- [46] Y. Borodko, P. Ercius, V. Pushkarev, C. Thompson, G. Somorjai, *J. Phys. Chem. Lett.* **2012**, *3*, 236–241.
- [47] N. C. Bigall, T. Hartling, M. Klose, P. Simon, L. M. Eng, A. Eychmüller, *Nano Lett.* **2008**, *8*, 4588–4592.
- [48] J. M. Zhang, F. Ma, K. W. Xu, *Appl. Surf. Sci.* **2004**, *229*, 34–42.
- [49] G. Ouyang, C. X. Wang, G. W. Yang, *Chem. Rev.* **2009**, *109*, 4221–4247.
- [50] A. Pimpinelli, J. Villain, *Physics of Crystal Growth*, Cambridge University Press, Cambridge, **1998**.
- [51] D. J. Smith, A. K. Petfordlong, L. R. Wallenberg, J. O. Bovin, *Science* **1986**, *233*, 872–875.
- [52] Y. J. Xiong, A. R. Siekkinen, J. G. Wang, Y. D. Yin, M. J. Kim, Y. N. Xia, *J. Mater. Chem.* **2007**, *17*, 2600–2602.
- [53] X. M. Lu, M. Rycenga, S. E. Skrabalak, B. Wiley, Y. N. Xia, *Annu. Rev. Phys. Chem.* **2009**, *60*, 167–192.
- [54] B. Wiley, T. Herricks, Y. G. Sun, Y. N. Xia, *Nano Lett.* **2004**, *4*, 1733–1739.
- [55] T. S. Ahmadi, Z. L. Wang, T. C. Green, A. Henglein, M. A. ElSayed, *Science* **1996**, *272*, 1924–1926.
- [56] H. Lee, S. E. Habas, S. Kweon, D. Butcher, G. A. Somorjai, P. D. Yang, *Angew. Chem.* **2006**, *118*, 7988–7992; *Angew. Chem. Int. Ed.* **2006**, *45*, 7824–7828.
- [57] Y. J. Xiong, Y. N. Xia, *Adv. Mater.* **2007**, *19*, 3385–3391.
- [58] B. W. Lim, X. M. Lu, M. J. Jiang, P. H. C. Camargo, E. C. Cho, E. P. Lee, Y. N. Xia, *Nano Lett.* **2008**, *8*, 4043–4047.
- [59] S. I. Lim, I. Ojeda-Jimenez, M. Varon, E. Casals, J. Arbiol, V. Puntes, *Nano Lett.* **2010**, *10*, 1970–1970.
- [60] J. Zhang, J. Y. Fang, *J. Am. Chem. Soc.* **2009**, *131*, 18543–18547.
- [61] H. Song, F. Kim, S. Connor, G. A. Somorjai, P. D. Yang, *J. Phys. Chem. B* **2005**, *109*, 188–193.
- [62] Y. J. Xiong, J. M. McLellan, J. Y. Chen, Y. D. Yin, Z. Y. Li, Y. N. Xia, *J. Am. Chem. Soc.* **2005**, *127*, 17118–17127.
- [63] Y. J. Xiong, H. G. Cai, B. J. Wiley, J. G. Wang, M. J. Kim, Y. N. Xia, *J. Am. Chem. Soc.* **2007**, *129*, 3665–3675.
- [64] N. R. Jana, L. Gearheart, C. J. Murphy, *J. Phys. Chem. B* **2001**, *105*, 4065–4067.
- [65] C. J. Murphy, N. R. Jana, *Adv. Mater.* **2002**, *14*, 80–82.

- [66] S. E. Habas, H. Lee, V. Radmilovic, G. A. Somorjai, P. Yang, *Nat. Mater.* **2007**, *6*, 692–697.
- [67] A. R. Tao, S. Habas, P. D. Yang, *Small* **2008**, *4*, 310–325.
- [68] B. Lim, M. J. Jiang, P. H. C. Camargo, E. C. Cho, J. Tao, X. M. Lu, Y. M. Zhu, Y. N. Xia, *Science* **2009**, *324*, 1302–1305.
- [69] M. S. Jin, H. Zhang, Z. X. Xie, Y. N. Xia, *Angew. Chem.* **2011**, *123*, 7996–8000; *Angew. Chem. Int. Ed.* **2011**, *50*, 7850–7854.
- [70] J. Y. Chen, T. Herricks, Y. N. Xia, *Angew. Chem.* **2005**, *117*, 2645–2648; *Angew. Chem. Int. Ed.* **2005**, *44*, 2589–2592.
- [71] T. Herricks, J. Y. Chen, Y. N. Xia, *Nano Lett.* **2004**, *4*, 2367–2371.
- [72] S. S. Cheong, J. D. Watt, R. D. Tilley, *Nanoscale* **2010**, *2*, 2045–2053.
- [73] J. W. Geus, J. A. R. van Ween, *Catalysis: An Integrated Approach to Homogeneous, Heterogeneous and Industrial Catalysis* (Eds.: J. A. Moulijn, P. W. N. M. van Leeuwen, R. A. van Santen), Elsevier, Amsterdam, **1993**, Chap. 9.
- [74] G. A. Somorjai, S. H. Joo in *Silica and Silicates in Modern Catalysis* (Ed.: I. Halasz), Transworld Research Network, Kerala, India, **2010**.
- [75] J. Y. Park, C. Aliaga, J. R. Renzas, H. Lee, G. A. Somorjai, *Catal. Lett.* **2009**, *129*, 1–6.
- [76] Y. Wan, D. Y. Zhao, *Chem. Rev.* **2007**, *107*, 2821–2860.
- [77] H. Song, R. M. Rioux, J. D. Hoefelmeyer, R. Komor, K. Niesz, M. Grass, P. D. Yang, G. A. Somorjai, *J. Am. Chem. Soc.* **2006**, *128*, 3027–3037.
- [78] F. Zaera, G. A. Somorjai, *J. Am. Chem. Soc.* **1984**, *106*, 2288–2293.
- [79] Q. Yuan, A. X. Yin, C. Luo, L. D. Sun, Y. W. Zhang, W. T. Duan, H. C. Liu, C. H. Yan, *J. Am. Chem. Soc.* **2008**, *130*, 3465–3472.
- [80] P. D. Yang, D. Y. Zhao, D. I. Margolese, B. F. Chmelka, G. D. Stucky, *Nature* **1998**, *396*, 152–155.
- [81] H. Tuysuz, Y. Liu, C. Weidenthaler, F. Schuth, *J. Am. Chem. Soc.* **2008**, *130*, 14108–14110.
- [82] Y. Ren, Z. Ma, L. P. Qian, S. Dai, H. Y. He, P. G. Bruce, *Catal. Lett.* **2009**, *131*, 146–154.
- [83] X. H. Sun, Y. F. Shi, P. Zhang, C. M. Zheng, X. Y. Zheng, F. Zhang, Y. C. Zhang, N. J. Guan, D. Y. Zhao, G. D. Stucky, *J. Am. Chem. Soc.* **2011**, *133*, 14542–14545.
- [84] Z. L. Wang, *J. Phys. Chem. B* **2000**, *104*, 1153–1175.
- [85] Y. W. Zhang, W. Y. Huang, S. E. Habas, J. N. Kuhn, M. E. Grass, Y. Yamada, P. Yang, G. A. Somorjai, *J. Phys. Chem. C* **2008**, *112*, 12092–12095.
- [86] G. A. Somorjai, S. K. Beaumont, S. Alayoglu, *Angew. Chem.* **2011**, *123*, 10298–10311; *Angew. Chem. Int. Ed.* **2011**, *50*, 10116–10129.
- [87] H. M. Zheng, R. K. Smith, Y. W. Jun, C. Kisielowski, U. Dahmen, A. P. Ali-visatos, *Science* **2009**, *324*, 1309–1312.
- [88] S. Cheong, J. Watt, B. Ingham, M. F. Toney, R. D. Tilley, *J. Am. Chem. Soc.* **2009**, *131*, 14590–14595.
- [89] G. A. Somorjai, C. Aliaga, *Langmuir* **2010**, *26*, 16190–16203.
- [90] S. Alayoglu, S. K. Beaumont, F. Zheng, V. V. Pushkarev, H. M. Zheng, V. Iablokov, Z. Liu, J. H. Guo, N. Kruse, G. A. Somorjai, *Top. Catal.* **2011**, *54*, 778–785.
- [91] F. Tao, M. E. Grass, Y. W. Zhang, D. R. Butcher, J. R. Renzas, Z. Liu, J. Y. Chung, B. S. Mun, M. Salmeron, G. A. Somorjai, *Science* **2008**, *322*, 932–934.
- [92] G. A. Somorjai, J. Y. Park, *Top. Catal.* **2008**, *49*, 126–135.
- [93] C. J. Kiewer, C. Aliaga, M. Bieri, W. Y. Huang, C. K. Tsung, J. B. Wood, K. Komvopoulos, G. A. Somorjai, *J. Am. Chem. Soc.* **2010**, *132*, 13088–13095.
- [94] G. A. Somorjai, H. Frei, J. Y. Park, *J. Am. Chem. Soc.* **2009**, *131*, 16589–16605.
- [95] M. Grass, R. Rioux, G. Somorjai, *Catal. Lett.* **2009**, *128*, 1–8.
- [96] C. J. Kiewer, M. Bieri, G. A. Somorjai, *J. Am. Chem. Soc.* **2009**, *131*, 9958–9966.
- [97] J. N. Kuhn, W. Y. Huang, C. K. Tsung, Y. W. Zhang, G. A. Somorjai, *J. Am. Chem. Soc.* **2008**, *130*, 14026–14027.
- [98] M. E. Grass, Y. W. Zhang, D. R. Butcher, J. Y. Park, Y. M. Li, H. Bluhm, K. M. Bratlie, T. F. Zhang, G. A. Somorjai, *Angew. Chem.* **2008**, *120*, 9025–9028; *Angew. Chem. Int. Ed.* **2008**, *47*, 8893–8896.
- [99] K. M. Bratlie, H. Lee, K. Komvopoulos, P. D. Yang, G. A. Somorjai, *Nano Lett.* **2007**, *7*, 3097–3101.
- [100] I. Lee, F. Delbecq, R. Morales, M. A. Albiter, F. Zaera, *Nat. Mater.* **2009**, *8*, 132–138.
- [101] I. Lee, R. Morales, M. A. Albiter, F. Zaera, *Proc. Natl. Acad. Sci. USA* **2008**, *105*, 15241–15246.
- [102] F. Zaera, *Acc. Chem. Res.* **2009**, *42*, 1152–1160.
- [103] S. Alayoglu, C. Aliaga, C. Sprung, G. A. Somorjai, *Catal. Lett.* **2011**, *141*, 914–924.
- [104] S. H. Joo, J. Y. Park, C. K. Tsung, Y. Yamada, P. D. Yang, G. A. Somorjai, *Nat. Mater.* **2009**, *8*, 126–131.
- [105] C. A. Witham, W. Y. Huang, C. K. Tsung, J. N. Kuhn, G. A. Somorjai, F. D. Toste, *Nat. Chem.* **2010**, *2*, 36–41.
- [106] G. A. Somorjai, F. Tao, J. Y. Park, *Top. Catal.* **2008**, *47*, 1–14.
- [107] J. Y. Liu, *ChemCatChem* **2011**, *3*, 934–948.

Received: April 12, 2012

Published online on August 27, 2012